2025-01-5079 Published 09 Dec 2025

SAE INTERNATIONAL

Real-time Analysis of Battery Degradation in a Plug-in Hybrid Electric Vehicles during Vehicle-to-Grid Operation

Laxman Timilsina, Ali Moghassemi, Elutunji Buraimoh, Ali Arsalan, S.M. Imrat Rahman, Grace Muriithi, Gokhan Ozkan, Behnaz Papari, and Christopher S. Edrington Clemson University

Citation: Timilsina, L., Moghassemi, A., Buraimoh, E., Arsalan, A. et al., "Real-time Analysis of Battery Degradation in a Plug-in Hybrid Electric Vehicles during Vehicle-to-Grid Operation," SAE Technical Paper 2025-01-5079, 2025, doi:10.4271/2025-01-5079.

Received: 16 Sep 2025 Revised: 18 Nov 2025 Accepted: 18 Nov 2025

Abstract

This paper examines the effect of vehicle-to-grid (V2G) integration on battery aging and the economic viability of plug-in hybrid electric vehicles (PHEVs). Due to their energy storage potential, V2G technologies are considered an environmentally friendly means to increase the stability of power grids. Persistent V2G operations tend to reduce battery lifetime and, consequently, will increase its replacement cost, which is a source of uncertainty for EV owners. This work investigates battery degradation under two scenarios: first, under normal vehicle operation using the US06 drive cycle, and second, under V2G operation with a 10-kW and 15-kW bidirectional charger. In the case of V2G operation, the charger discharges the battery by 20 kWh and then recharges it back to 90% state of charge (SoC) at a constant 1C-rate. Real-time simulations are performed in order to validate these results: a grid, a bidirectional charger, and the vehicle battery are modeled in a real-time simulator; furthermore, a pair of controllers is used in order to run the energy management and predict the battery aging. Economic analysis assesses the capacity loss due to V2G participation as well as the incentives, providing a comprehensive view of the economic feasibility of V2G applications and their potential benefits.

Keywords

Battery degradation, Hybrid electric vehicle, Electric vehicle, Vehicle-to-grid, Energy management

1. Introduction

The increased popularity of electrified vehicles can be justified due to variable costs and large environmental impacts resulting from nonrenewable sources. Both electric vehicles (EVs) and plug-in hybrid electric vehicles (PHEVs) have the tendency to alleviate some environmental problems, as opposed to conventional ICE-based vehicles. Among the available batteries in the market, lithium-ion batteries can be considered the most promising and preferred choice for future generations [1]. These batteries have several advantages that make them superior compared to others for EVs: higher energy density allows driving a longer range with improved performance, higher power density, and good high-temperature performance. Besides, lithium-ion batteries are lighter and more compact than other types of batteries, which improves the total vehicle efficiency and aids in designing [1, 2].

For a long time, batteries have been the favorite choice for utilities when it comes to energy storage. However, the high prices of the batteries have made it difficult to install them on a large scale [2]. Recently, the sales of EVs have boomed, and their batteries are now being used for other purposes, like supporting the grid, besides just being used for propulsion [3, 4]. The concept of using the battery's power to supply the grid or support the grid is known as vehicle-to-grid (V2G) technology, where a smart charging strategy allows the batteries to supply power to the grid and vice versa. Hence, the batteries with high capacity used in EVs in this approach are not only used for powering EVs but also as a backup supply for the electrical grid. Apart from V2G, the other important terminologies related to bidirectional discharging are V2X, which stands for vehicle-to-everything. V2X includes applications ranging from V2H (vehicle to home), V2B (vehicle to building) up to V2L (vehicle to load) services [3]. Such applications increase the role and prospects of vehicle batteries being used as something more than just a traveling battery.

From a utility perspective, V2G has several benefits. V2G provides flexibility and active energy storage to secure the grid from even more dimensions. Utilities can use it to smooth fluctuations in demand by compiling energy storage resources of many attached EVs. When demand is low, power from the grid can be used to charge the EV batteries, thus balancing the supply and demand of power. These dispersed energy storage units, represented by EVs, will provide the flexibility to improve grid resilience and reliability for the grid without investing in expensive additional energy storage facilities [5, 6]. In addition, with large battery capacities, EVs can even serve as backup power to homes in emergency situations, integrated as V2H systems. Furthermore, the V2G technology enables the smooth integration of renewable energy sources into the grid. When a huge amount of energy is produced due to the excess generation of renewable sources, batteries in EVs can store such energy and sell it to the grid when the renewable generation is less. This can help maintain the grid frequency and voltage [7, 8].

Through participation in the V2G schemes, EV owners are able to generate incentives through the sale of energy from their vehicle batteries to the grid during peak hours and recharging during off-peak hours. Incentives will not only create financial rewards but also stabilize the grid. According to [9], these incentives were found to be between \$650 and \$1575 in California and from \$525 to \$1575 in the United Kingdom, per year for EV owners using their vehicles as a source of income through V2G. Some owners in Sweden have earned between \$30 and \$655 each year. Furthermore, [10] mentions that a Nissan LEAF, equipped with a 15-kW bidirectional charger, economized \$793.28 over 5 months by V2G operations; this translates to a potential incentive of \$1900 annually. These savings can further be optimized using a higher power rating bidirectional chargers.

However, all of these incentives do not consider the cost of the battery's degradation. As the battery is one of the critical and expensive elements in EVs/PHEVs, its degradation cost should be included in V2G incentive calculations. If this cost is not considered in the V2G strategies, the incentive calculation can generate a misleading conclusion about the actual benefit, as the battery pack is one of the most expensive components of the vehicle. For this reason, battery degradation should be considered to carry out a realistic economic evaluation during V2G operation.

Few research papers have included detailed assumptions while modeling battery aging in V2G applications. For example, in the study [11], one decentralized optimal scheduling approach for EVs was proposed to prolong battery lifetime by suggesting keeping the state of charge (SoC) between 20% and 85%. Study [12] focused on the integration of renewable energy through coordination in charging and discharging of EVs within certain predefined limits to minimize battery degradation, studying the effect of different current magnitudes for charging/discharging. There is a research gap with respect to studying the economic viability of the operations of an EV in the context of both V2G functionality and normal driving use, considering the costs associated with battery degradation. The following research tries to fill this knowledge gap by providing a techno-economic analysis of the V2G application along with a thorough battery deterioration model for both normal vehicle usage and V2G connection.

2. Statement of Contribution

There is limited research on precisely forecasting battery aging during both regular and V2G operation of a vehicle. In order to fill this research gap, this study develops a data-driven degradation model using artificial neural network (ANN) techniques to enable accurate forecasting of battery degradation used in EVs/PHEVs.

Furthermore, a realistic simulation scenario is developed that includes vehicle operation for both normal driving and V2G operation. This simulation serves as a solid foundation for testing and validating the predictions of the deterioration model in real-world settings. To evaluate the economic implications for EV owners, a numerical simulation of the battery is carried out using MATLAB/Simulink, with consideration given to battery degradation. To further validate these findings, a real-time experiment is conducted using a simulation setup involving the grid, bidirectional charger, and vehicle battery modeled in Typhoon, a digital real-time simulator (DRTS). The energy management of the vehicle is deployed in a Raspberry Pi, while another Raspberry Pi serves as a controller for predicting battery degradation. These controllers and simulators communicate via CAN communication. Based on the results obtained from these simulations, an economic analysis is done to assess whether the incentives from V2G operation justify the potential costs associated with battery degradation. Furthermore, the study compares the predicted end of life (EOL) of the battery under regular vehicle operation versus the application of the vehicle with V2G operation, highlighting the impact of regular connection of the vehicle to V2G on the battery lifetime.

The remaining paper is divided into the following sections: Section 3 provides the detailed architecture of the vehicle and bidirectional charger considered in this study. Section 4 explains the modeling technique used to predict battery aging. Section 5 elaborates on the real-world simulation strategy of the vehicle used in this study. Section 6 presents the simulation results. Section 7 presents the economic analysis based on the findings from Section 6. Finally, Section 8 presents the conclusion of the paper and directions for future research.

3. Bidirectional Charger and PHEV Architecture Modeling

The system considered in this study is shown in Figure 1. The vehicle's battery is connected to the grid through a bidirectional charger and a grid-forming transformer. In this configuration, there is an AC/DC converter in the bidirectional charger, which converts the AC energy from the grid into DC energy. Directly after this converter, there is a bidirectional DC/DC converter that is directly connected to the EV/PHEV battery. The modeling of these converters in the figure is based on study [13]. The system parameters considered are highlighted in Table 1, which are taken into account during modeling. As for the control strategy, the paper mainly focuses on the DC bus voltage of the V2G system. Therefore, this paper has adopted a widely adopted double PI control strategy with a voltage outer loop and current inner loop. A decoupling scheme for the grid voltage feedforward has been introduced to improve the stability of the system. In addition, the modeling of this converter is explained in detail in studies [13, 14], respectively.

TABLE 1 System parameters.

Parameters	Value
Grid voltage (RMS)	230 V
Grid-side filter inductance	0.9 mH
Resistor	0.1 Ω
DC bus filter capacitor	12,000 μF
DC inductance	0.2 mH
DC capacitor	1000 μF
DC bus voltage	600 V
Battery voltage	400 V
Grid frequency	50 Hz

3.1. Architecture of the Vehicle

The usage of PHEVs is increasing due to their ecologically friendly transportation option that utilizes more than one power source; often, at least one provides electric power for propulsion to an electric motor. The PHEVs fall into a number of categories depending on the type of energy sources and the architecture of power delivery. The most common in this regard is a type that combines an engine and a battery to supply the vehicle's demanded power. A series PHEV architecture is used in this study due to its simple design with flexibility in implementing control actions.

In a series hybrid configuration, the engine does not directly power the vehicle but runs a generator that converts its output into electricity. The converted electrical energy is utilized either to charge the battery or to supply the power to drive the motor. This arrangement provides easier control to implement power delivery to the vehicle wheel, hence simplifying traction control. The advancement in power electronics has significantly improved the efficiency and reliability of PHEVs [15]. This architecture enables high fuel efficiency, low emissions, and more control of the power distribution to the wheels. Decoupling of the ICE from the drivetrain allows for more

FIGURE 1 Overall system diagram considered in this study.

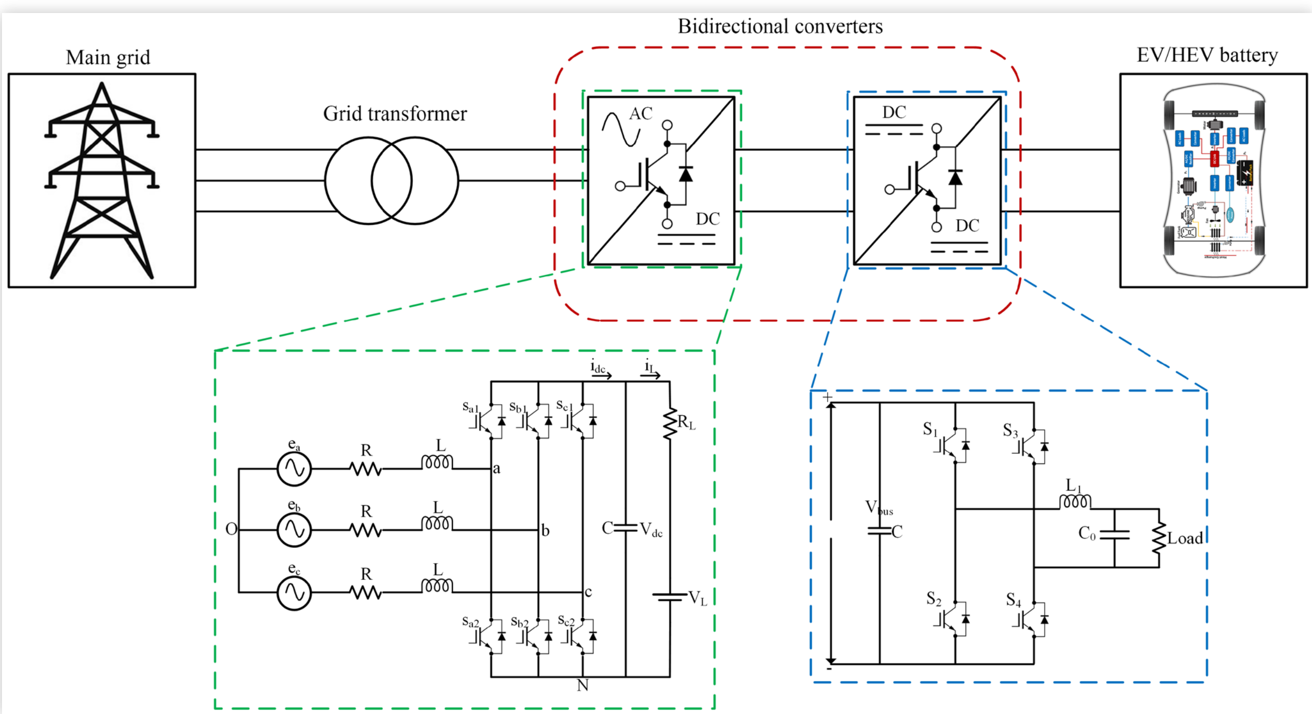

FIGURE 2 PHEV architecture used in this study.

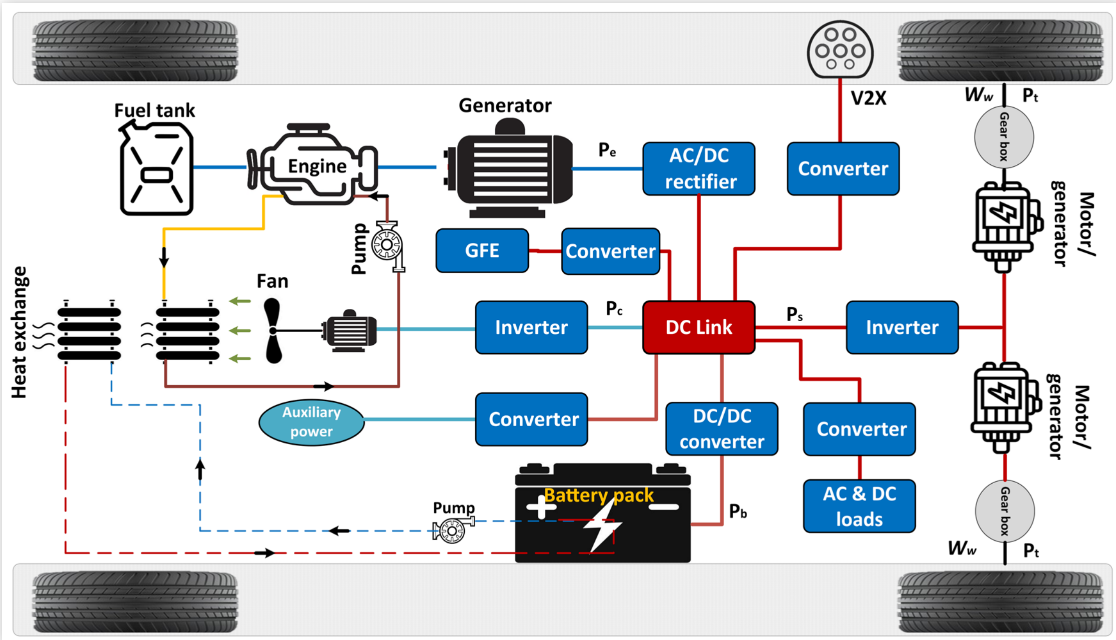

flexible control strategies and further simplifies traction management [16].

In this subsection, the electrical model of the PHEV considered in this study is elaborated. The model includes a 600 V DC bus powered by both an engine and a battery. A battery capacity of 73 kWh and an engine rating of 180 kW are used in this study. As illustrated in Figure 2, the vehicle architecture uses power electronics converters to separate the energy sources and loads from the bus. This segmentation helps to implement an EMS and mitigates power distribution challenges commonly encountered in PHEVs. This modeling further supports V2G and V2V functionality through a V2X outlet, which is considered in this research. The detailed vehicle parameters necessary for the calculation of reference power during a defined driving cycle are considered from the study [17].

The battery considered in this study is modeled by connecting 2.9 Ah 18,650 NCA cells in series and parallel configurations to achieve a nominal terminal voltage of 400 V and a capacity of 182 Ah. With a nominal voltage of 3.6 V, a capacity of 2.9 Ah, and an energy content of 10.44 Wh, to achieve the target terminal voltage, 112 cells are connected in series, while 63 such series strings are connected in parallel and meet the desired capacity of 73 kWh. This configuration results in a total of 7056 individual cells in the complete battery pack. The specific choice of 2.9 Ah NCA cells during the modeling of the battery is for the accurate prediction of battery degradation. In Section 4, this paper leverages data from laboratory testing of 2.9 Ah NCA cells to develop a degradation forecasting model using a neural network [18].

4. Battery Degradation Modeling and Forecasting

EV operation depends on the safety and reliability of the battery. Lithium-ion batteries age and degrade over time, which lowers the battery capacity and driving range. Battery states, driving behavior, charging circumstances, and environmental conditions are some factors that influence battery aging [19]. Hence, degradation abatement through accurate degradation modeling and optimizing battery usage is important to maximize the EV lifespan. However, it is difficult to identify the causes of degradation, which makes it difficult to develop a degradation model.

In automotive applications, the battery life cycle is much shorter compared to other expensive components, and furthermore, the operation of the vehicle is considered unreliable below 80% of the initial capacity [16]. The complex aging mechanisms require understanding and are very crucial for economic viability and extending the life of the batteries. Factors like temperature, discharge, charge currents, or DoD have different influences on the capacity of a battery [1]. All these factors, collectively or individually, will cause various types of stresses for EV batteries during operation, and they must be considered when modeling or predicting the degradation path.

Recently, ANNs have become popular as one of the strongest tools for modeling complicated systems and data-driven predictions. They mathematically mimic the activity of the neurons of the brain by using interconnected neurons. Neural networks make predictions by learning from data provided to them. At the center of the networks are neurons that serve as a fundamental unit that processes input data and generates output. Neurons are connected by weighted connections, creating a network. Information is transferred between neurons, which is processed and forwarded to other neurons [20]. In order to predict the battery's deterioration path, a neural network–based degradation model is developed in this study. ANN is chosen due to its ability to model complex, nonlinear relationships between multi-dimensional input features and battery degradation. This is particularly useful when degradation behavior is not explicitly captured by empirical equations. Additionally, ANN models are more scalable to new data than traditional lookup-based or rule-based models.

This paper develops a three-layer neural network that can be used for the prediction of battery capacity loss. It consists of an input layer, a hidden layer, and an output layer (Figure 3). Preprocessing is done, and necessary features such as voltage, current, temperature, and capacity are extracted to feed into the model. Three distinct inputs are fed into the network's input layer: temperature, voltage, and current. The output layer, however, is in charge of forecasting the battery's capacity. There is only one hidden layer in the architecture, and it has 32 neurons. The rectified linear unit (ReLU) function is used for this layer as the activation function since ReLU is a popular choice for hidden layers of a neural network; it enables the model to learn complex nonlinear relationships that give better performance boosts in prediction. Finally, the output layer consists of only one neuron since the regression task aims to predict the capacity loss of the battery. No activation function is specified for the output layer to ensure it gives raw output values that directly represent the predicted continuous output. The data is then divided into distinct sets that can be used for training, testing, and validation, each serving its purpose in the predictive model as shown by (1).

FIGURE 3 The architecture of the neural network used in this study.

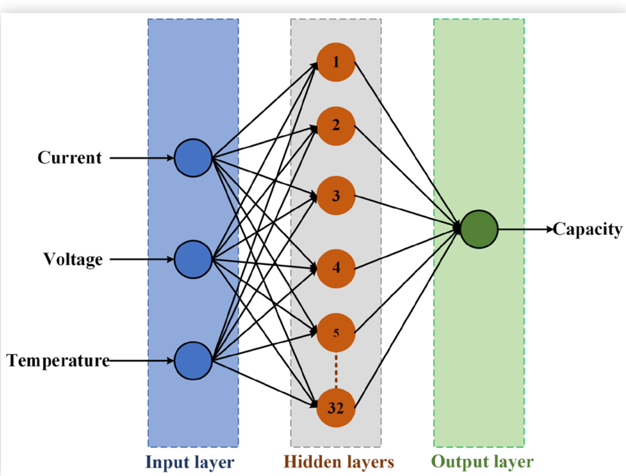

$$\delta_{train} = \left[\left(x_1, Y_1\right), \left(x_2, Y_2\right), \ldots, \left(x_n, Y_n\right)\right] \quad (1a)$$

$$\delta_{test} = \left[\left(x_{n+1}, Y_{n+1}\right), \left(x_{n+2}, Y_{n+2}\right), \ldots, \left(x_s, Y_s\right)\right] \quad (1b)$$

$$\delta_{validation} = \left[\left(x_{s+1}, Y_{s+1}\right), \left(x_{s+2}, Y_{s+2}\right), \ldots, \left(x_t, Y_t\right)\right] \quad (1c)$$

where x and Y are the filtered dataset extracted from the raw data. Here x contains the input parameters to the NN, namely voltage, current, and temperature, as $x_i = (V_i, i_i, T_i)$. Also, Y is the output obtained from the neural network that represents the battery's capacity. The NN is trained using δ_{train}, while the model created using train data sets is tested and validated using δ_{test} and $\delta_{validation}$ (Table 2).

Mean squared error (MSE) and the Adam optimizer are used to compile the neural network model. The MSE used as a loss function estimates the average of the squared differences in magnitude, one between the forecasted and another between the original output values. Adam optimizer is one of the most popular optimization algorithms, updating model parameters according to the calculated gradient values during training. Adam is an optimization algorithm that extends stochastic gradient descent to handle non-convex problems in efficient ways [21, 22]. It provides faster convergence and needs fewer computational resources compared to other optimization methods. Specifically, Adam performs best under conditions involving large datasets since it keeps more accurate gradients for several iterations in a row during the learning process [21]. In this way, by combining two other stochastic gradient methods, namely adaptive gradients and root mean square propagation, Adam provides a learning method that is optimal for many NNs.

An adequate amount of historical data is necessary to train the neural networks. In this study, the dataset provided by the University of Wisconsin-Madison is used, which provides the data for 2.9 Ah Panasonic 18,650 PF cells [18]. To improve the accuracy of the study, the cell data is scaled up to the 73 kWh battery pack. Multiple aging tests conducted at five different temperatures included in this dataset are used: 25°C, 10°C, 0°C, −10°C, and −20°C [18]. For each temperature, 10 individual drive cycle datasets were used, resulting in a total of 50 drive

TABLE 2 Hyperparameters for the selected neural network.

Parameters	Values
Input parameters	3
Hidden layers	1
Neurons	32 (LSTM cells)
Output parameter	1
Epoches	100
Learning rate	0.001
Optimizer	Adam
Loss function	MSE

FIGURE 4 Battery aging dataset available at five different temperatures used to train the neural network.

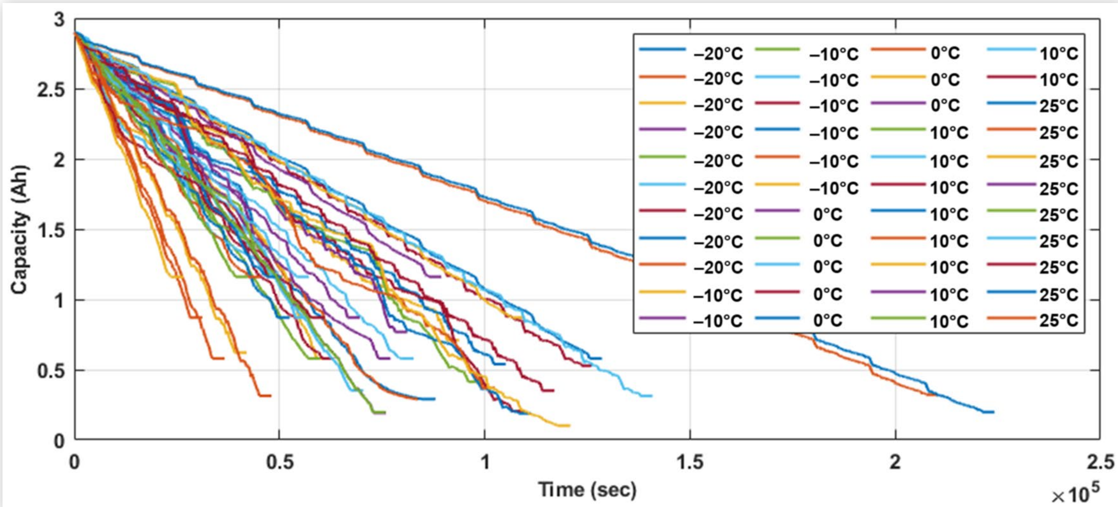

cycles. From these, this study extracted 315,752 individual data points. These samples were split as follows:

- Training: 70% (221,026 samples)
- Validation: 15% (47,363 samples)
- Testing: 15% (47,363 samples)

All these datasets were used in the neural networks' training, testing, and validation process. Four distinct parameters—voltage, current, temperature, and battery cell capacity—are taken out of this dataset during preprocessing in order to train the neural network. Figure 4 shows the trends in the aging data for each drive cycle for five different temperatures.

The data shown in Figure 4 is used during the training, testing, and validation processes, except for one specific dataset during the modeling of the neural network. The fitting of the designed neural network during the training phase gave the following results: a mean absolute error (MAE) of 0.0789, MSE of 0.0129, and R-square of 0.9743. The battery cell data that was not included during the training and testing was used to predict the capacity loss with the trained neural network. For this unseen data, the fitting was found to have an MAE of 0.0816, MSE of 0.0212, and an R-square of 0.9556 and is shown in Figure 5.

In prior work [16], a Markov chain–based model was used to predict battery degradation. While effective in capturing discrete transition probabilities, it was limited in modeling complex nonlinear relationships. In this study, a neural network–based model is adopted for enhanced flexibility and accuracy. A detailed comparison of the Markov and neural network approaches can be found in [23], and is omitted here to maintain brevity.

It is important to note that the neural network model used in this study was trained on temperature data

FIGURE 5 Battery aging prediction using trained neural network.

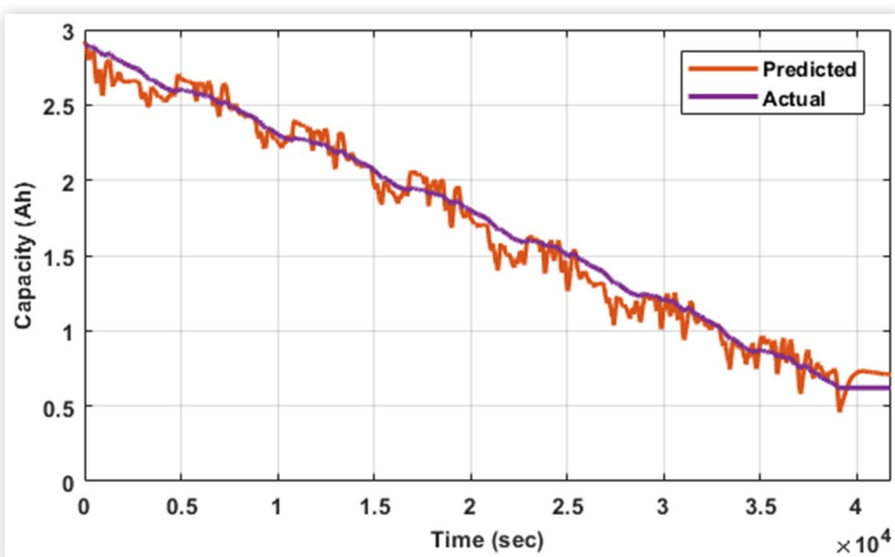

ranging only from –20°C to 25°C. Therefore, any degradation predictions for conditions exceeding 25°C are extrapolations beyond the training domain and remain unvalidated. Caution is advised when applying this model to high-temperature automotive environments, especially during summer operation or in hot climates. Also, the neural network model used in this study is based on degradation data from 18,650 cells tested under controlled conditions and is scaled to a 73 kWh pack under the following assumptions:

- All cells behave identically,
- Pack capacity loss is equivalent to per-cell loss, and
- Thermal gradients and cell-balancing inefficiencies are negligible.

These assumptions simplify the modeling but do not reflect real-world variations in temperature, cycling conditions, or cell-level manufacturing deviations. As such, the predictions may underestimate localized or uneven degradation that occurs in large battery packs.

5. Analysis of Operation of PHEV

There are two different, distinct cases in which the aging of the battery used for V2G operations can arise. First, it is possible to have degradation during normal vehicle operation, that is, degradation from vehicle driving. Second, there is degradation that may be specifically attributed to the V2G connection itself due to frequent vehicle charging and discharging.

For the normal operation of the vehicle, a standard drive cycle (US06) is utilized to simulate the driving scenario. In contrast, for the V2G operation, the rating of the charger determines the rate of degradation. Here, two ratings of the charger are considered: a 10 kW and a 15 kW bidirectional charger. In this V2G connection for a 10 kW charger, the battery undergoes a 2-hour discharge followed by charging the battery back to a predefined SoC. The following subsections explain in detail the degradation mechanism under these two scenarios.

5.1. Degradation under Normal Vehicle Operation

To realistically simulate under driving conditions, a PHEV is considered, which operates for an average national distance of about 12,000 miles [24]. This is simulated by using a standard driving profile, US06, that covers a distance of 8.01 miles per cycle. With four driving cycles on an average day, the vehicle covers a total distance of 11,695 miles per year, fairly close to the national average in the U.S.

In a PHEV with more than one power source, an EMS is necessary [25, 26]. The aim of the EMS is to distribute optimized power among the sources present in the vehicle. There are two sources of power for the PHEV considered in this study: the engine and the battery. The objective of the EMS is to allocate the power among these sources so as to minimize the overall fuel consumption [27]. Therefore, the power that the battery will supply could be different from the total power that the vehicle requires. Because of this, the degradation of the battery will depend on how much it supplies power during the operation of the vehicle [28]. In this work, an EMS explored in the studies [16, 29] has been adopted for the research. A further elaboration of this EMS and how it functions within the context of power-sharing between the engine and the battery in the PHEV is explained in detail as follows.

5.1.1. Energy Management The EMS can be represented by (2), which uses an optimization function aimed at minimizing fuel cost.

$$\min \sum_{s\in\mathcal{S}} f_s\left(P_s\left(t_k\right)\right) \tag{2a}$$

$$P_s\left(t_k\right) \in \mathcal{P} \tag{2b}$$

where t_k is the time instant in the discrete domain, $\mathcal{S}$ is the set of indices of energy sources, $P_s(t_k)$ is the power generated by source s at t_k, and $\mathcal{P}$ is the corresponding constraint set of $P_s(t_k)$.

The vehicle's fuel consumption depends upon the power supplied by the ICE (P_{ICE}). This cost can be minimized through the EMS, as depicted in (2a) and is represented in quadratic form, as shown in (3):

$$f_s\left(P_{ICE}\right) = c^F\left(\alpha_s\left(P_{ICE}\right)^2 + \beta_s P_{ICE} + \gamma_s\right), \quad \alpha_s > 0 \tag{3}$$

where c^F ($/gallon) represents the cost of fuel, P_s is the power supplied by the ICE during vehicle operation, α_s is the quadratic term in the cost function, which is a positive parameter ($\alpha_s > 0$) that determines the concavity of the cost function. For a high α_s value, the weight of the quadratic term in the cost function becomes greater, and then, the optimization process becomes sensitive to the deviations from desired reference powers. The coefficients β_s reflect the linear terms within the cost function in relation to the way reference powers drive the cost of P_s. The β_s herein weighs the contribution of the linear term in the cost function and can either be positive or negative, which either favors a particular power split or penalizes it in the case that the actual split is different from some desirable split. And finally, γ_s is the constant term in the cost function. It accounts for any other expenses or gains from the power division not represented by the quadratic or linear terms.

The cost coefficients in Equation 3 are adapted from the benchmark EMS presented in [16], and are used to model the fuel consumption behavior of the ICE in the

TABLE 3 Cost function coefficients used in the EMS optimization. (Date taken from Ref. [16].)

Parameter	Value	Unit
α_s	0.00052	\$/kW²
β_s	0.0152	\$/kW
γ_s	0.65	\$

PHEV. These parameters are listed in Table 3 with their units.

The EMS optimization function is modeled as a constrained optimization problem. These include constraints such as the power-generating limits of sources in a vehicle, the total load demanded, and the SoC of a battery. The sequential quadratic programming (SQP) algorithm is used in order to solve this optimization problem. This is an iterative method derived for nonlinear programming problems in solution with constraints. It mainly aims at finding the minimum or maximum of the objective function while maintaining all defined constraints throughout the iteration process.

Besides these, there are other constraints that are considered, as mentioned in (2b). Every power source has a limit to its generation capacity, which is considered one of the constraints for the EMS. (2b) represents the minimum and maximum generation limits as

$$\underline{P_{bat}} \le P_{bat} \le \overline{P_{bat}} \tag{4a}$$

$$\underline{P_{ICE}} \le P_{ICE} \le \overline{P_{ICE}} \tag{4b}$$

The powertrain has to supply all the loads properly. The total power generated by the sources must meet the total load demanded and any other associated losses. With this a power supply and demand constraint (5) can be formed as follows.

$$P_{bat} + P_{ICE} = P_{AC\ load} + P_{DC\ load} + P_{propulsion} + P_{V2X} + P_{loss} \tag{5}$$

where P_{bat} is power generated by the battery, P_{ICE} is power generated by the ICE, $P_{AC\,load}$ is AC load, $P_{DC\,load}$ is DC load, which are not considered in this study, $P_{propulsion}$ is propulsion load, P_{V2X} is power used for V2X mode, and P_{loss} is the total loss.

Each system has its own internal constraints, as stated in (6). The components considered in this study are the ICE and battery; hence following constraints are assumed for these power-generating sources.

$$|P_{ICE}(t_{k+1}) - P_{ICE}(t_k)| < rr_{ICE} \tag{6a}$$

$$\left|P_{bat}(t_{k+1}) - P_{bat}(t_k)\right| < rr_{bat} \tag{6b}$$

$$\underline{SoC_{bat}} \le SoC_{bat} \le \overline{SoC_{bat}} \tag{6c}$$

$$SOC_{bat}(t_{k+1}) = SOC_{bat}(t_k) - \frac{\delta T i_{bat}}{Q_{nom}} \tag{6d}$$

where $\delta T = t_{k+1} - t_k$. Constraints (6a) and (6b) represent the ramp rates for the battery and the ICE, respectively. Constraints (6c) and (6d) are the battery's constraints, where Q_{norm} is the nominal capacity of the battery. (6c) represents the boundary level of the SoC of the battery, and (6d) represents the SoC calculation of the battery using the Coulomb counting method. Also, P_{bat} is defined as positive when the battery is discharging (supplying power to the system) and negative when charging, including during regenerative braking events. The SoC update in (6d) accounts for both directions of current flow via Coulomb counting. Therefore, regenerative braking is inherently modeled as part of the power flow from the vehicle to the battery.

For economic efficiency, the EMS particularly focuses on fuel consumption and tries to minimize it by allocating more power to the battery when it's possible. The sharing of the optimized power between the sources is shown in Figure 6. Now, the amount of power supplied by the battery allocated from this EMS is utilized for calculating its aging.

5.2. Degradation of Battery under V2G Operation

Depending on the particular application, a bidirectional charger at the substation or at home is necessary to implement a V2G connection. The bidirectional charges for the V2G connection are available at different ratings: 7 kW, 10 kW, and 15 kW, with 10 kW being the most frequently used one [30]. The aging effect of V2G on EV's battery and its long-term viability are two major concerns for EV owners. An EV typically draws 20 kW of power when cruising and over 100 kW of power when accelerating from the battery [31]. On the other hand, an EV used for V2G application draws much less constant power from the battery, making it experience less stress, stay cool, and drain slowly. Furthermore, V2G usually lasts for 2–4 hours, which discharges or charges the battery slowly with less impact on aging. An average EV battery capacity (typically 60 kWh) is usually three times more than the average household load and six times more than a household battery (10 kWh) [31]. If a 10 kW bidirectional charger is used for 2 hours, then only 20 kWh energy is extracted from the battery, which doesn't impact the battery significantly. A simulation is run in light of these considerations in order to examine how V2G affects a PHEV's battery.

In this work, the simulation of V2G connection is based on a common working day in order to capture precisely the battery discharge and charge cycle for a V2G operational cycle. It is assumed that on a normal working day profile, the PHEV owner drives to the office, parks in a V2G-enabled location, and drives home later. The following points highlight various instances of a day for this V2G operation:

1. **Vehicle arrives and is connected for V2G operation:** Upon arrival at the workplace, the PHEV is connected to the V2G port. For this study, the battery starts with a SoC above 80%.

FIGURE 6 Optimized power allocated to ICE and battery by the EMS.

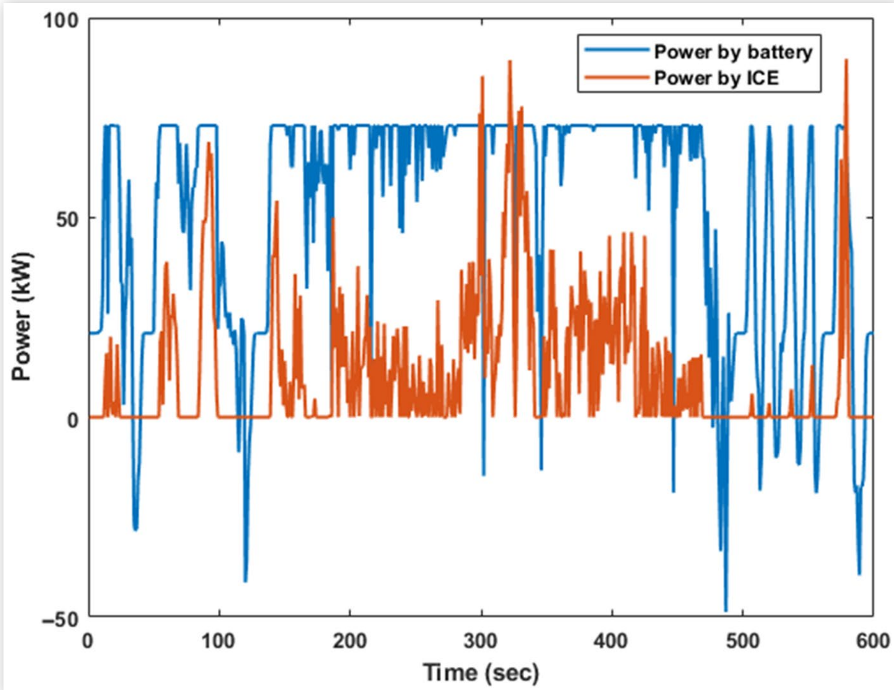

2. **Controlled discharge of the battery:** The battery is discharged using a bidirectional charger for 2 hours at a rate of 1 C-rate. The process stops when the SoC reaches 40% or after 2 hours, whichever comes first. This ensures the battery remains healthy during V2G operation and minimizes degradation.
3. **Recharging of the battery:** After discharge, the battery is charged back up to 90% SoC using the same 1 C-rate. The entire discharge and recharge cycle takes approximately 4 hours, which aligns with a typical workday and ensures the vehicle is ready for the return commute.

This simulation scenario reflects a realistic daily routine for a PHEV owner and their V2G participation. It considers both the driving distance covered and the time needed for charging and discharging.

The degradation cost associated with V2G operation is calculated using (7). The factor 0.2 in the equation accounts for the limited usable capacity in EV applications (the usable range is typically between 100% and 80% of its initial capacity). The capacity loss of the battery is calculated by the developed neural network, and the initial cost of the battery is considered to be $151 per kWh [32]. Also, to analyze the impact of charger capacity, this study analyzes two V2G scenarios:

- In the first scenario, a 10 kW bidirectional charger is used.
- In the second scenario, a 15 kW charger is used.

Finally, battery degradation under these two charging conditions is measured and compared.

$$\text{Cost of degradation} = \text{Initial cost} * \frac{\text{Capacity loss}}{0.2} \tag{7}$$

6. Simulation Results

6.1. MATLAB/Simulink Simulation

This section explains the results obtained from the simulation conducted in MATLAB/Simulink. Among several loads considered in vehicle operations, the propulsion load is typically the most significant. As US06 is used as a reference drive cycle in this study, Figure 7 illustrates the propulsion load for the vehicle considered in this study. This simulation scenario represents a high-energy-throughput use case (approximately 4 US06 cycle, which equals 32 miles), aligning with EPA commute averages of 30–40 miles per day for U.S. drivers [24]. The US06 cycle is a high-power, high-speed profile that approximates aggressive acceleration, short bursts, and highway conditions. While this may not fully reflect all real-world usage patterns, it provides a useful stress-testing baseline for battery degradation assessment.

To analyze the aging of the battery on a PHEV, a simulation is conducted as explained in Section 5. First, the vehicle is driven for two drive cycles, which account for the commuting distance from home to the office. The power to be supplied from the battery is obtained from the EMS for this operating condition, as discussed in Section 5.1.1, and the power allocation to the ICE and battery is shown in Figure 6. From this figure, the power

FIGURE 7 Propulsion power demanded by the PHEV for the US06 drive cycle.

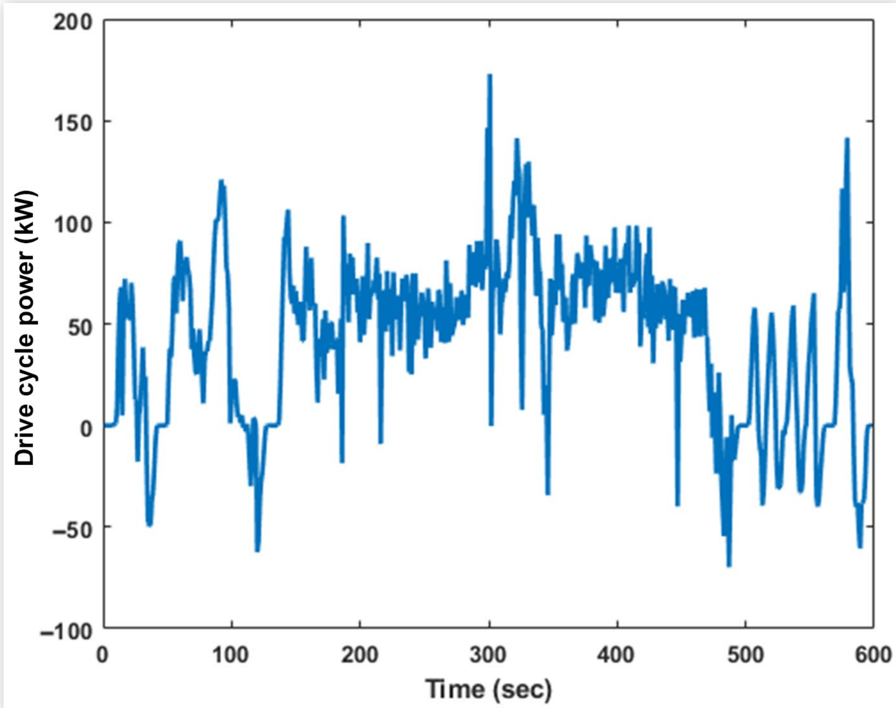

allocated to the battery by the EMS is used to calculate the battery degradation. After this, in the simulation, the vehicle is now connected for the V2G operation using a 10 kW bidirectional charger. For the first 2 hours, 20 kWh of energy is discharged from the battery, followed by charging the battery until it reaches 90% SoC.

The sequence of operation is shown in Figure 8, which shows the degradation path of the battery simulated for a week. During each day (shown by the zoomed-in area within the red box), as explained above, the vehicle follows a pattern. First, it operates for two drive cycles, which takes about 20 minutes. It then plugs into a V2G system for about 4 hours before it enters another two drive cycles, running for another 20 minutes. This figure shows that the aging rate of the battery is higher when the vehicle is driving under a US06 drive cycle than under a V2G connection. This can be attributed to the fact that the battery is under more stress when the vehicle is accelerated in its operation, which means increased degradation. On the other hand, during the V2G link, the battery undergoes less stress with the extraction of just 20 kWh at a slow rate for 2 hours each. Therefore, degradation during this phase is relatively low. Thus, the vehicle is on for an average of 4.7 hours a day, and the resulting battery degradation path over the course of the seven days is shown in Figure 8.

6.2. Real-time Simulation

For validation of the results obtained from the MATLAB/Simulink experiment using real-time simulators and multiple controllers, an experiment in real-time is conducted as shown in Figure 9. Real-time simulation is conducted for more accurate validation of controller logic under hardware constraints and better representation of system dynamics and latency. Equipment from Clemson's Real-time Control and Optimization Laboratory (RTCOOL) is utilized, where a Typhoon HIL 606 simulator is used as DRTS and the Raspberry Pis as controllers. In the following sections, a detailed description of real-time implementation and experimental results is presented.

6.3. System Modeling

The system shown in Figure 1 is developed using a schematic editor in Typhoon control center software. This model is then compiled and integrated into the HIL SCADA system before being deployed into the DRTS Typhoon HIL 606.

The control algorithms for the EMS are usually deployed on a control unit, usually known as an electronic control unit (ECU), in vehicles. Here, a Raspberry Pi 4 Model B serves as the ECU responsible for running the algorithm of the EMS. Also, the optimization problem for the objective function of the EMS is solved using an IPOPT solver within the Pi. In addition, the degradation prediction model was developed as explained in Section 4, which is based on a neural network, runs on another controller. The requisite Python code for degradation prediction is deployed on this controller.

Now, the real-time operational data from the system (Typhoon) is transmitted to the Raspberry Pis, where the first Pi executes the EMS algorithm to determine the optimal reference power levels to be provided by the

FIGURE 8 Degradation path of battery simulated for 7 days.

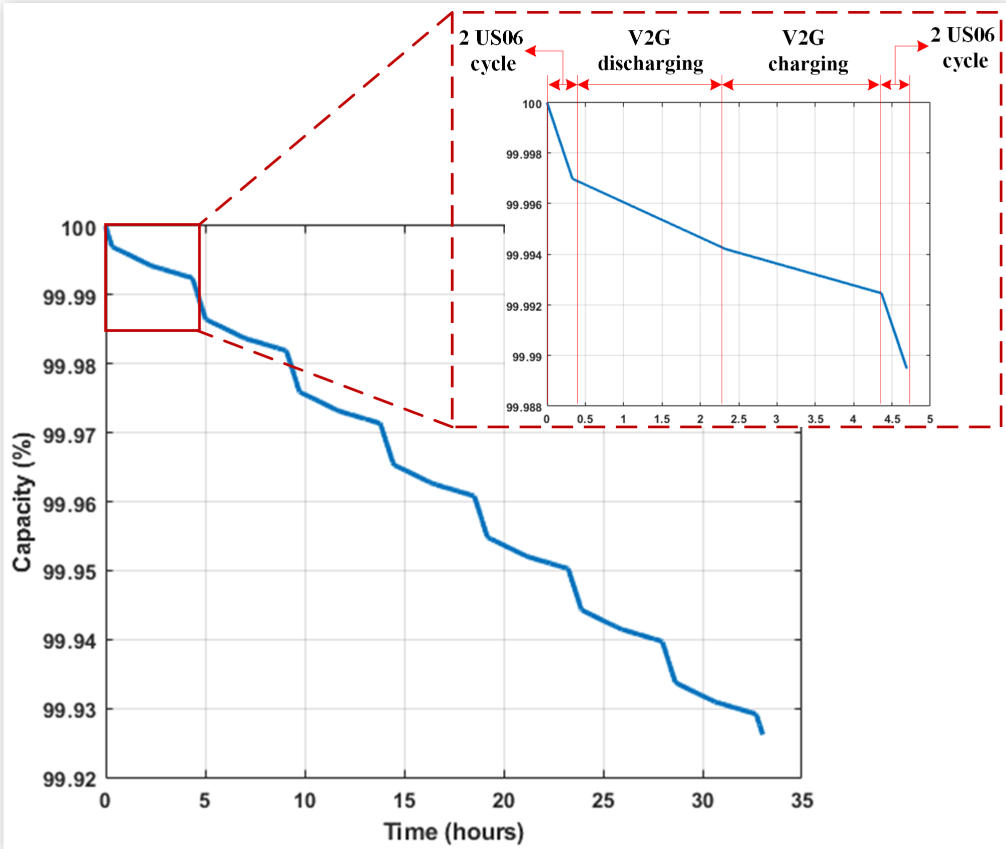

FIGURE 9 Real-time implementation of the system.

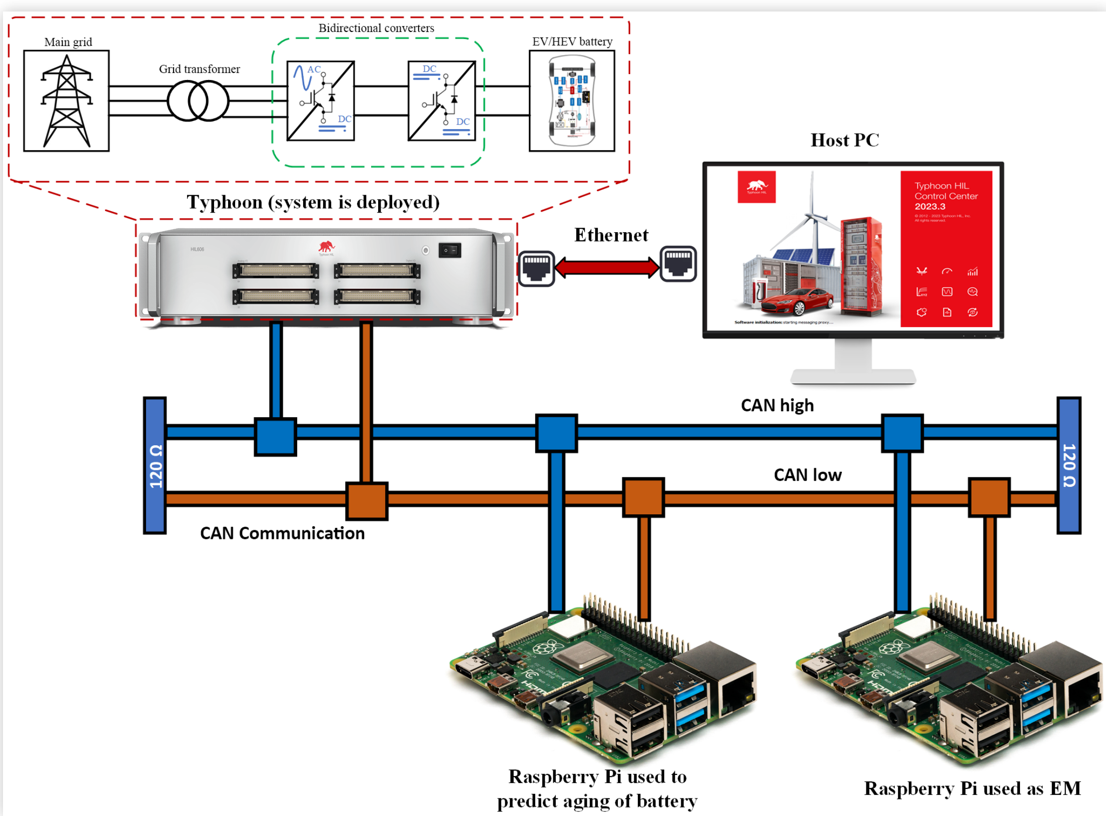

FIGURE 10 HMI screen for visualization.

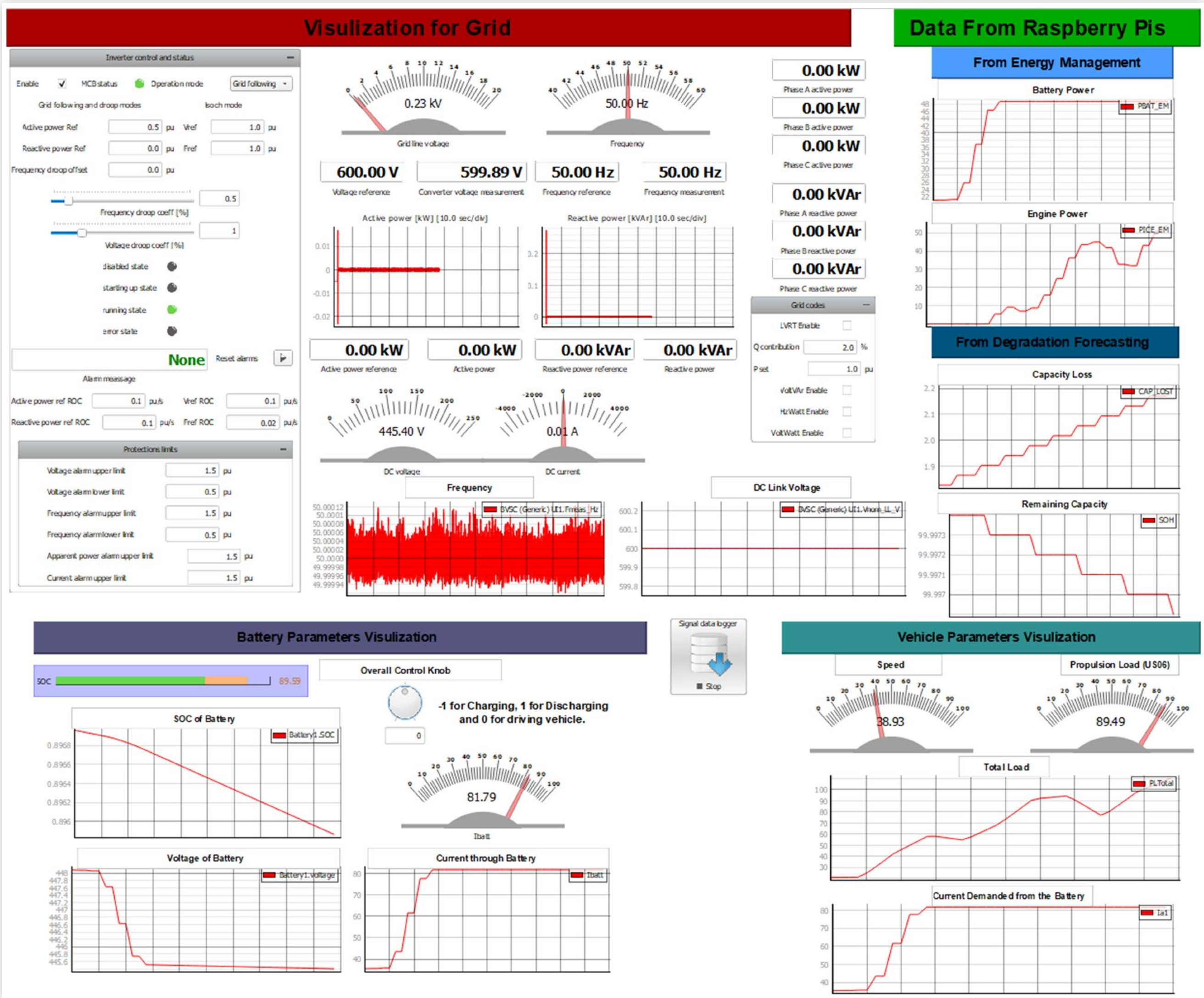

battery and the ICE. Subsequently, these reference power values are relayed back to the Typhoon system. Now, the battery power to be supplied is used to predict the degradation of the battery, which is forwarded to another Raspberry Pi to predict the degradation. The result from this degradation prediction model is the capacity loss and the remaining capacity or state of health (SoH) of the battery, which are sent back to the Typhoon and are visualized using an HMI screen, as shown in Figure 10. Since the EMS and the degradation prediction algorithm are all deployed in the vehicle itself and in automotive applications, controller area network (CAN) communication is the standard communication protocol used. Therefore, for this study, CAN communication is utilized to facilitate data exchange between the simulator and the ECUs.

The real-time operation data is sent from Typhoon to the Raspberry Pis. One of the Pis runs an EMS algorithm that allocates the optimal reference power to the battery and ICE. These optimal values are sent back to the Typhoon system. Simultaneously, the power allocated to the battery is used to predict the battery degradation, managed by another Raspberry Pi. The degradation prediction model outputs—battery capacity loss and SoH—are relayed to Typhoon and displayed on an HMI screen as shown in Figure 10.

In automotive applications, both the EMS and degradation prediction algorithms are implemented within the vehicle itself. In automotive applications, CAN is the standard communication protocol. Hence, CAN communication is used in this study to support seamless data exchange between the simulator and ECUs, as shown in Figure 9.

6.4. Visualization

The human–machine interface (HMI) for system monitoring utilizes a HIL SCADA window integrated into the Typhoon control center, supplemented by a Python visualization environment. Operational data from diverse sources, including the simulator and all ECUs, is gathered by the Typhoon system and displayed within the SCADA window.

The HMI comprises four main sections:

- Grid Visualization: Displays grid line voltage, frequency, reference active power set for bidirectional charger, and actual active power flow through the grid.
- Battery Parameters Visualization: Shows SoC, terminal battery voltage, and current through the battery.
- Vehicle Parameters Visualization: Illustrates speed, total power demanded by the vehicle, and current demanded by the vehicle from the battery.
- Raspberry Pis Data Visualization: Presents data from two Raspberry Pis:
  - The first Raspberry Pi shows data from the EM, including power allocated to the engine and battery.
  - The second Raspberry Pi displays the total capacity lost during regular vehicle and vehicle-to-grid (V2G) operations, along with the remaining battery capacity.

6.5. Experimental Results

Figure 10 shows the results obtained from the CHIL experiment, which graphically presents the real-time screen results for both Case I and Case II. The results of these two cases are explained in detail in the following two subsections. For instance, in normal driving conditions, the vehicle runs through four US06 drive cycles, which will lead to a certain amount of battery degradation even though the vehicle isn't in a V2G mode. Figure 11(a) shows the battery capacity loss when the vehicle is driven normally without a V2G connection, whereas Figure 11(b) shows the daily variation in battery capacity.

FIGURE 11 Real-time simulation result for (a) capacity loss, (b) SoH of battery for 4 US06 drive cycles.

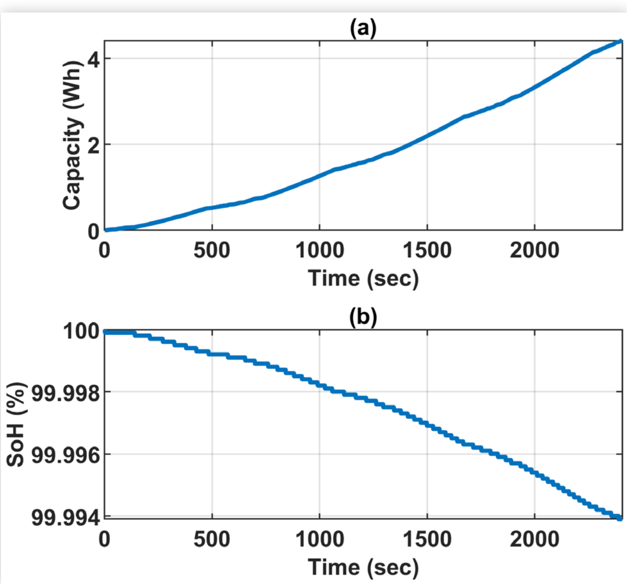

6.5.1. Case I

To understand how different ratings of bidirectional chargers influence battery degradation, this study investigates two distinct cases with varying charger ratings. For one of these scenarios, a 10 kW bidirectional charger is employed. The purpose of this simulation is to observe how the battery degradation evolves, specifically during V2G operations, which involve the vehicle's battery supplying power back to the grid and the battery being charged. Figures 12–15 provide the results for this case.

The daily variation in SoC of the battery is illustrated in Figure 12. The simulation commences at 90% SoC, with the vehicle being operated over two US06 drive cycles. The initial decrease in SoC during the first 1200 sec is attributed to these two drive cycles. Following this, the vehicle is connected to the V2G system to discharge the battery for a duration of 2 hours to discharge 20 kWh. The subsequent recharging of the battery back to 90% takes longer than the discharge period, as depicted in the

FIGURE 12 SoC variation of the battery for a day.

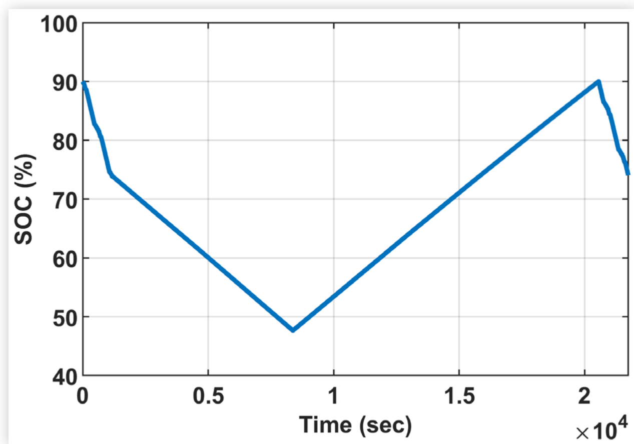

FIGURE 13 Voltage variation of the battery for a day.

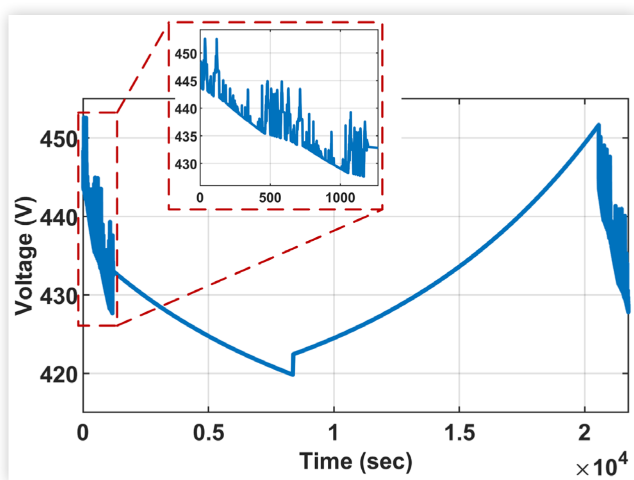

FIGURE 14 Current variation of the battery for a day.

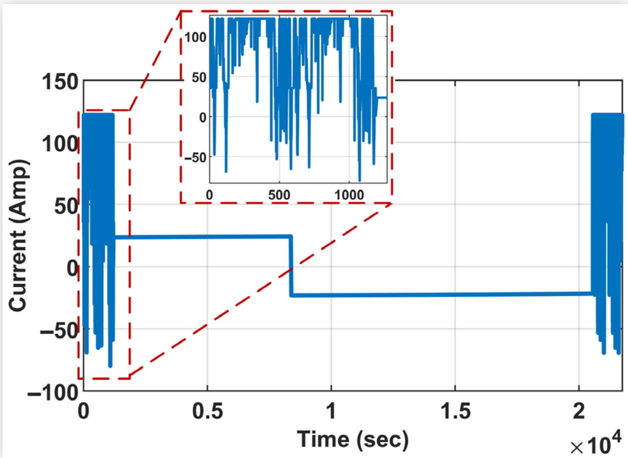

FIGURE 15 Real-time simulation result for (a) capacity loss, (b) SoH of battery during a day.

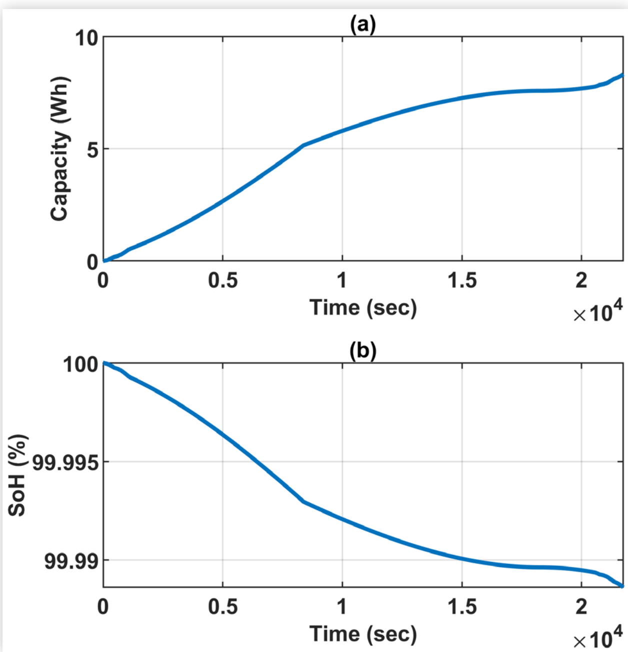

figure. The vehicle, after recharging, again undergoes two US06 drive cycles, which also lead to a further SoC decline from 90%. This pattern is repeated the following day. The result shows that the SoC declines faster during the US06 drive cycles than the discharge rate during V2G operation with a 10 kW charger. This phenomenon occurs because the energy demand from the battery during driving conditions exceeds the power discharged during the V2G connection.

The variation in the terminal voltage of the battery throughout the simulation is illustrated in Figure 13. During the initial and final 1200 sec, the fluctuations in terminal voltage are attributable to the vehicle's operation over two US06 drive cycles, resulting in both discharging and charging of the battery, which causes corresponding increases and decreases in terminal voltage. Following the initial 1200 sec, a decline in terminal voltage is observed as the battery connects to the V2G system and discharges for a duration of 2 hours. Subsequently, a rise in terminal voltage occurs, reflecting the charging of the battery while in V2G connection mode.

The pattern of the current supplied by the battery throughout the simulation is illustrated in Figure 14. During the initial and final 1200 sec, the fluctuations in current are attributable to the vehicle's operation over two US06 drive cycles, resulting in both discharging and charging of the battery. Following the initial 1200 sec, around 24 A [obtained using (5)] of nearly constant current is discharged to supply power to the grid for V2G operation. Again, during the charging condition, the grid supplies a nearly constant current of around 23 A to charge the battery.

The current supplied by the battery throughout the simulation is depicted in Figure 14. During the first and last 1200 sec, the current fluctuations are due to the vehicle's operation over two US06 drive cycles, leading to both discharging and charging of the battery. After the initial 1200 sec, a steady discharge of approximately 24 A (calculated using Equation 8) occurs to supply power to the grid during V2G operation. Similarly, during the charging phase, the grid provides a nearly constant current of around 23 A to recharge the battery.

$$\text{Current} = \frac{\text{Power rating}}{\text{Terminal voltage}} \tag{8}$$

The capacity loss of the battery and the variation in SoH during the simulation, which incorporates both the drive cycle and V2G operation, are illustrated in Figure 15(a) and (b), respectively. Figure 15(a) presents the capacity loss during vehicle operation, measured in watt-hours (Wh), while the SoH of the battery is derived from the loss using (9). The total capacity of the battery is 73 kWh, and the capacity loss is predicted by the Raspberry Pi functioning as ECU-2, utilizing a neural network as discussed earlier. The neural network predicts that the total capacity lost in one day after the vehicle has been driven for four US06 drive cycles and undergone discharging and charging through V2G operation is 8.317 Wh. This corresponds to a capacity loss of 0.0114%. Consequently, the SoH, calculated using Equation 9, is found to be 99.9886%.

$$\text{SOH}(\%) = \frac{\text{Total capacity (Wh)} - \text{Capacity loss (Wh)}}{\text{Total capacity (Wh)}} \tag{9}$$

6.5.2. Case II In this scenario, a 15 kW charger is employed, in contrast to the 10 kW charger used in Case I. The same simulation as in Case I is conducted to assess the impact of the higher-rated charger on battery degradation. The results indicate that the patterns of SoC and voltage are

FIGURE 16 Current variation in the battery for a day in Case II.

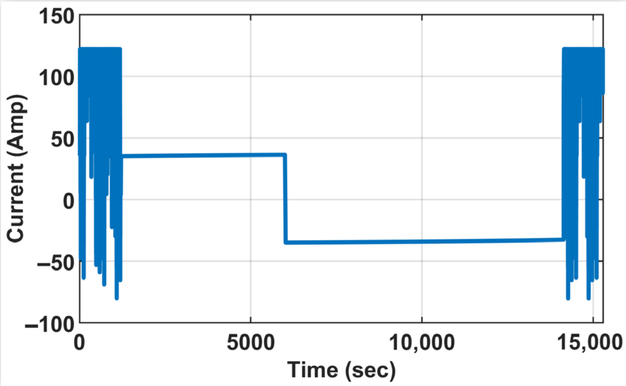

nearly identical to Figures 12 and 13, although there are some variations in instantaneous values due to the charger's rating (not shown over here). Figure 16 illustrates the current flowing through the battery throughout the simulation for a day. Notably, when compared to Figure 14, the waveforms for the first and last 1200 sec are similar, as the vehicle operates using US06 drive cycles. However, after 1200 sec, the battery supplies a nearly constant current of approximately 36 A (depending on terminal voltage) during discharging, and −35 A during charging from the grid. These current levels are higher than those in Case I due to the use of a higher rating of a bidirectional charger.

Similarly, the capacity loss of the battery and the variation in SoH during the simulation, which includes both the drive cycle and V2G operation, are depicted in Figure 17(a) and (b), respectively. Figure 17(a) presents the

FIGURE 17 Real-time simulation result for (a) capacity loss, (b) SoH of battery during a day.

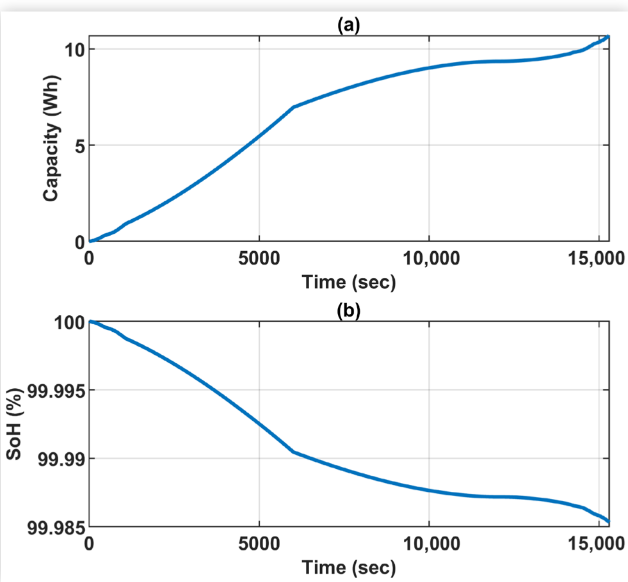

capacity loss during vehicle operation, measured in watt-hours (Wh), while the SoH of the battery is calculated from this loss using (9). The neural network predicts that the total capacity lost in one day, after the vehicle has been driven for four US06 drive cycles and has undergone discharging and charging through V2G operation using a 15 kW charger, is 10.6383 Wh, which corresponds to a capacity loss of 0.0145%. Consequently, the SoH, as determined by Equation 9, is 99.9854%. This increased degradation is attributed to the higher C-rate associated with both the charging and discharging processes. The degradation mechanisms related to varying C-rates are detailed in the study [1].

7. Economical Analysis

The capacity loss of the battery under two distinct simulation environments, with and without a V2G connection, is shown in Table 4. An economic analysis is conducted for a 10 kW bidirectional charger to compare real-time results with those from the numerical simulations presented in the study [33]. The first four rows of Table 4 present the findings from the study [33], while the last four rows, highlighted in gray, showcase the real-time results. From the results of the numerical simulation in a week, the vehicle with a V2G connection had a slightly higher capacity loss of 0.0738% compared to the vehicle without a V2G connection, which had a capacity loss of 0.042%. If this result is scaled up for a year, the vehicle without a V2G connection is expected to have a capacity loss of 2.184%. This would result in a degradation cost of $1203.75. Similarly, the vehicle with a V2G connection has a higher capacity loss of 3.83%. This capacity loss leads to a degradation cost of $2110.9. Hence, from this data, it can be concluded that the battery used in a vehicle with a V2G connection needs replacement faster compared to a vehicle without a V2G application. The vehicle without a V2G connection needs battery replacement after approximately 9 years, whereas the vehicle with a V2G connection requires a replacement of battery after around 5 years. Figure 18 shows the battery degradation path of the vehicle under these two conditions: with and without

TABLE 4 Battery degradation under normal vehicle operation (without V2G) and with V2G application.

	Without V2G	With V2G
Degradation in a week (NS)	0.042%	0.0738%
Degradation in a year (NS)	2.184%	3.83%
Cost of degradation per year (NS)	$1203.75	$2110.9
Battery age until EOL (NS)	9.16 years	5.22 years
Degradation in a week (RT)	0.044%	0.0798%
Degradation in a year (RT)	2.29%	4.16%
Cost of degradation per year (RT)	$1262.48	$2293.41
Battery age until EOL (RT)	8.7 years	4.8 years

FIGURE 18 Comparison of battery degradation path with and without V2G connection for two simulation environments.

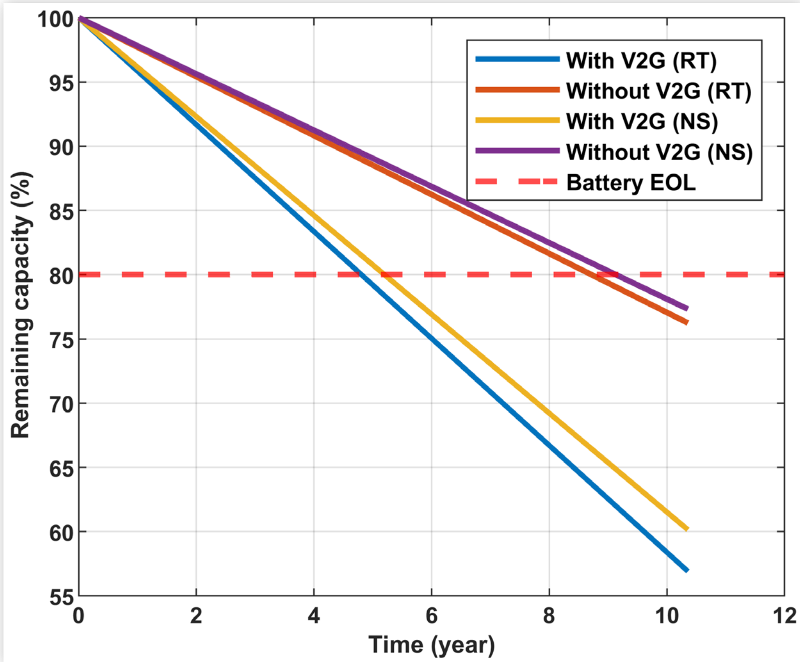

a V2G connection for both MATLAB/Simulink, named as numerical simulation (NS) and real-time (RT). This figure confirms the observation discussed earlier regarding the battery's EOL. Both simulation results exhibit the same trend, with minor discrepancies arising from differences in the simulation environments.

Similarly, under the RT simulation, the result is almost similar, with small variations. Over a week, the capacity loss of the battery was found to be 0.044% for a vehicle without a V2G connection. Similarly, the vehicle with V2G has a higher capacity loss of 0.0798%. Again, if this result is scaled up for a year, the vehicle without a V2G connection will have a capacity loss of 2.29%, and the vehicle with a V2G connection will have 4.16% of capacity loss. This results in the degradation cost of $1262.48 and $2293.41 for the vehicle without V2G and with V2G connection, respectively. Again, from the capacity loss of the battery, it can be concluded that the battery used in a vehicle without a V2G connection needs replacement after approximately 8.7 years, whereas the battery used in a vehicle with a V2G connection requires replacement after around 4.8 years.

For the V2G application, if the EV owner sells 20 kWh of stored energy back to the utility, it must go through a conversion process. The DC power has to be converted back to AC using an inverter, and this process incurs an efficiency loss of around 10%. Thus, the energy available for sale to the utility by the EV owner at the moment of connection is lowered to 18 kWh. In contrast, a rectifier with an efficiency loss of roughly 10% facilitates the conversion from AC power to DC during battery charging. With 20 kWh of usable energy, the EV owner must pay for 22 kWh of AC power to properly charge the battery.

7.1. Case I: Maximum Benefit

The EV owner can maximize incentives by buying energy during off-peak hours and selling it back to the utility during peak hours. For this, the real electricity rate provided by Pacific Gas and Electric Company (PG&E) is considered for the analysis [34]. The potential for incentives occurs when EV owners can sell power or energy back to the utility during peak demand periods, when electricity prices are higher. This selling opportunity allows EV owners to take advantage of favorable market conditions, earning revenue by providing stored energy from their vehicle batteries to the grid. The rates offered by PG&E, as shown in Figure 19 are used in this study to do the economical analysis [34].

For maximum benefit, EV owners can sell the stored energy during these peak periods. The buying price (which is the price the utility pays to EV owners) is 64 cents per kWh. These prices are higher in order to provide an incentive for energy flow into the grid at those times when it is needed most—a factor for mutual benefit between the utility and the EV owner.

On the other hand, the utility also sells electricity back to consumers at different rates, and the off-peak hour price is used here for maximum benefit. These selling rates (the price EV owners pay when they purchase electricity to charge their vehicles) are lower than the buying rates during peak hours. The selling price during peak hours is 28 cents per kWh. Table 5 summarizes these key buying and selling rates for vehicles connected to V2G systems, providing a clearer picture of the potential benefits for EV owners who engage in energy transactions with the utility.

FIGURE 19 Electricity rates considered for economic analysis. (Data taken from Ref. [34].)

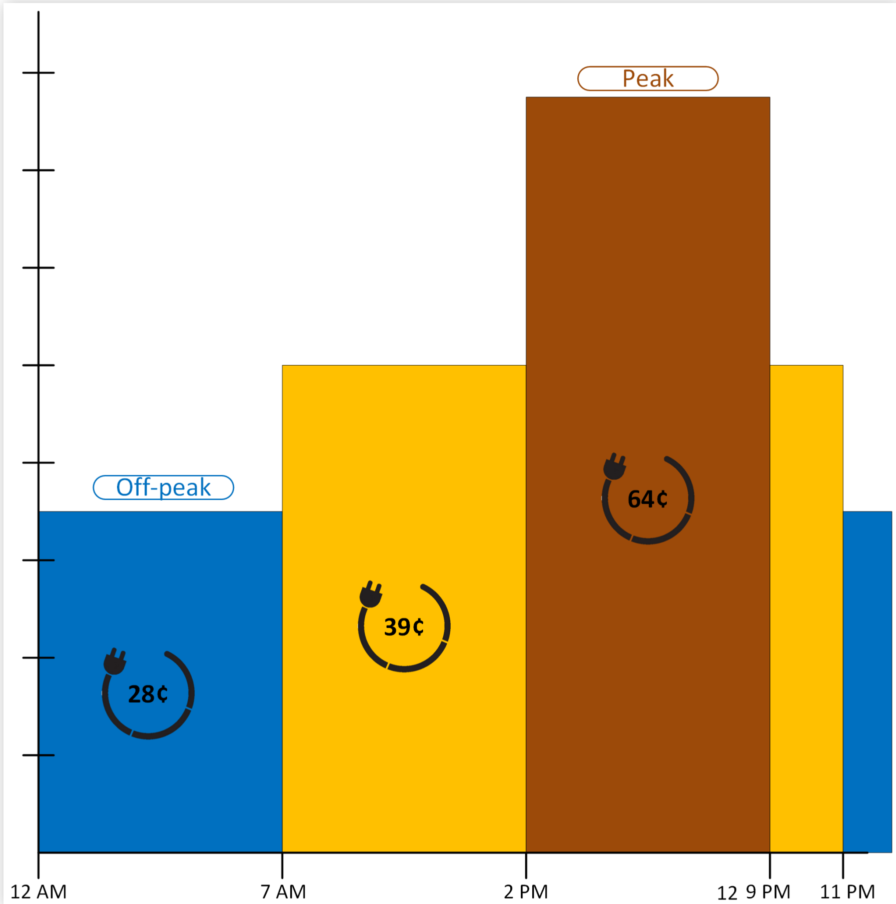

TABLE 5 Electricity buying and selling rate for V2G connection for maximum benefit. (Data taken from Ref. [34].)

	Buying	Selling
Energy (kWh)	22	18
Rates	$0.28	$0.64
Cost for a year	$2248.4	$4204.8
Saving	$1956.4	

The economic analysis assumes a fixed time-of-use (TOU) pricing model, where the vehicle discharges energy during peak hours and recharges during off-peak periods. While this provides a clear contrast between V2G and non-V2G economics, we acknowledge that real-world pricing structures may include dynamic tariffs, demand charges, or net metering limits, which could affect profitability.

It is inferred from Table 5 that employing a V2G connection could save an electric vehicle owner up to $1956.4 in a year, which is essentially what one can earn by supplying only 20 kWh of electrical energy to the grid in one day. It goes without saying that sharing more energy during the time of the V2G connection boosts further potential savings.

The battery needs to be replaced after about 4.8 years of continuous use if the EV owner chooses to connect the vehicle to a V2G network. They will, however, also get an incentive of about $9390 during that time. It's worth noting that from this V2G connection, the EV owner needs to replace the battery after 4.8 years, as predicted from Table 4, but they will have $9390 as an incentive from V2G, which will cover almost 85% of the total battery cost, which is $11,023. However, if the owner of the EV chooses not to connect to V2G, the battery would require replacement without any incentives after 9.16 years, as predicted by the battery's degradation path (Table 4).

7.2. Case II: Normal Benefit

Achieving maximum benefit from buying and selling electricity is not always guaranteed. It may not always be feasible to purchase electricity during off-peak hours and sell it during peak hours at favorable rates. To account for this variability, a simplified assumption is made in this analysis. Instead of strictly considering off-peak and peak-hour dynamics, as illustrated in Figure 19, it is assumed that electricity is purchased at a standard rate of 39 cents per kWh and sold at peak-hour rate of 64 cents per kWh.

This approach is applied over a year to provide an average estimation, balancing the effects of non-peak purchases and peak-hour sales. Based on this assumption,

TABLE 6 Electricity buying and selling rate for V2G connection for normal benefit. (Data taken from Ref. [34].)

	Buying	Selling
Energy (kWh)	22	18
Rates	$0.39	$0.64
Cost for a year	$3131.7	$4204.8
Saving	$1073.1	

the results in Table 6 show that the total savings over 1 year amount to $1073.10. Extrapolating this value over 4.8 years—the expected EOL of the battery—results in cumulative savings of $5150.68.

Furthermore, the high-temperature conditions are not assumed in this study, and for instance, continuous operation near 40°C—the degradation rate may approximately double based on Arrhenius law. Under such conditions, the annual capacity loss could increase significantly from 2.2% to more than 4%, which would reduce the battery lifespan by nearly half and significantly alter the cost-benefit ratio of V2G participation.

Based on the data from Table 5, it can be concluded that an EV owner can save up to $1956.4 over the course of a year using a V2G connection. This is the total saving obtained by supplying 20 kWh of energy into the grid daily. By sharing more energy during a V2G connection, the potential savings can be increased even more.

The EV owner must replace the battery after about 5.22 years of continuous use if they choose to connect to the V2G network. On the other hand, they will also get an incentive of about $10,212 during that time. It's important to note that this V2G setup will result in battery degradation expenses of approximately $4735, yielding a net savings of approximately $5477 after 5.22 years. However, if the owner of the EV chooses not to connect to V2G, the battery will need to be replaced without any incentives after 9.16 years, as predicted by the battery's degradation path.

8. Conclusion

This paper offers a thorough analysis of PHEV battery degradation from two different perspectives: under normal vehicle operation and under V2G connection along with the normal operation of the vehicle. For the first one, the power supplied by the battery to calculate the capacity loss is determined by the EM, and consequently, the capacity loss is determined by the degradation forecasting model developed using the neural network. The study's second focus explores battery degradation under V2G connections, evaluating capacity loss through a predefined sequence of events using a data-driven method that uses neural networks.

The simulation of the vehicle is developed as a real-world scenario and is validated through two different simulation environments: MATLAB/Simulink and real-time simulation using Raspberry Pi as controllers and Typhoon as a DRTS. Finally, an economic analysis is conducted to find the maximum incentives that can be received from the V2G connection. Furthermore, this paper conducts an economical analysis considering the degradation cost of the battery and predicts the battery replacement time. In conclusion, this study provides EV owners with this comprehensive information, enabling them to make informed decisions on the use of V2G connections. Although these connections present attractive incentives, it's wise to be aware that they may shorten the battery lifetime and accelerate the battery replacement time.

While this study focuses on a specific PHEV configuration and a battery pack modeled using Panasonic NCR18650 cells, the proposed methodology is generalizable to other electric vehicle platforms and battery chemistries. The neural network degradation model can be retrained with cell data from different lithium-ion chemistries (e.g., NMC, LFP) to reflect their distinct degradation characteristics. Similarly, the vehicle model and energy management strategy are modular and can be adapted to full battery EVs (BEVs), hybrid architectures, or even stationary energy storage systems. Future work will explore these extensions to assess the broader applicability of V2G-enabled energy and degradation management across diverse EV platforms.

Contact Information

Laxman Timilsina
ltimils@clemson.edu

References

1. Timilsina, L., Badr, P.R., Hoang, P.H., Ozkan, G. et al., "Battery Degradation in Electric and Hybrid Electric Vehicles: A Survey Study," *IEEE Access* 11 (2023): 42431-42462.
2. Basel, J., Sapkota, N., Parekh, M., and Rao, A.M., "Electrolyte Optimization for Sodium-Sulfur Batteries," *Applied Physics Letters* 124, no. 12 (2024): 123901.
3. Liu, C., Chau, K., Wu, D., and Gao, S., "Opportunities and Challenges of Vehicle-to-Home, Vehicle-to-Vehicle, and Vehicle-to-Grid Technologies," *Proceedings of the IEEE* 101, no. 11 (2013): 2409-2427.
4. Buraimoh, E., Ozkan, G., Timilsina, L., Chamarthi, P.K. et al., "Overview of Interface Algorithms, Interface

Signals, Communication and Delay in Real-Time Co-Simulation of Distributed Power Systems," *IEEE Access* 11 (2023): 103925-103955.

5. Amamra, S.-A. and Marco, J., "Vehicle-to-Grid Aggregator to Support Power Grid and Reduce Electric Vehicle Charging Cost," *IEEE Access* 7 (2019): 178528-178538.
6. Gumrukcu, E., Arsalan, A., Muriithi, G., Joglekar, C. et al., "Impact of Cyber-Attacks on EV Charging Coordination: The Case of Single Point of Failure," in *2022 4th Global Power, Energy and Communication Conference (GPECOM)*, Nevsehir, Turkey, 2022, 506-511, IEEE.
7. Clement-Nyns, K., Haesen, E., and Driesen, J., "The Impact of Vehicle-to-Grid on the Distribution Grid," *Electric Power Systems Research* 81, no. 1 (2011): 185-192.
8. Buraimoh, E., Ozkan, G., Timilsina, L., Arsalan, A. et al., "Model Free Time Delay Compensation for Damped Impedance Method Interfaced Power System Co-Simulation Testing," SAE Technical Paper 2023-01-1600 (2023), doi:https://doi.org/10.4271/2023-01-1600.
9. Nuvve, "Nuvve Projects for V2G," accessed August 23, 2023, https://nuvve.com/projects/.
10. Fermata Energy, "Proven Results and Cost Savings with V2G Technology," accessed August 23, 2023, https://fermataenergy.com/article/proven-results-and-cost-savings-with-v2g-technology.
11. Xing, H., Fu, M., Lin, Z., and Mou, Y., "Decentralized Optimal Scheduling for Charging and Discharging of Plug-In Electric Vehicles in Smart Grids," *IEEE Transactions on Power Systems* 31, no. 5 (2015): 4118-4127.
12. Ahmadian, A., Sedghi, M., Mohammadi-ivatloo, B., Elkamel, A. et al., "Cost-Benefit Analysis of V2G Implementation in Distribution Networks Considering PEVS Battery Degradation," *IEEE Transactions on Sustainable Energy* 9, no. 2 (2017): 961-970.
13. Zhang, Z., Chen, R. et al., *Design of Three-Phase AC Power Electronics Converters* (Hoboken, NJ: John Wiley & Sons, 2023).
14. Han, J., Zhou, X., Lu, S., and Zhao, P., "A Three-Phase Bidirectional Grid-Connected AC/DC Converter for V2G Applications," *Journal of Control Science and Engineering* 2020, no. 1 (2020): 8844073.
15. Moghassemi, A., Rahman, S.I., Ozkan, G., Edrington, C.S. et al., "Power Converters Coolant: Past, Present, Future, and a Path toward Active Thermal Control in Electrified Ship Power Systems," *IEEE Access* 11 (2023): 91620-91659.
16. Timilsina, L., Hoang, P.H., Moghassemi, A., Buraimoh, E. et al., "A Real-Time Prognostic-Based Control Framework for Hybrid Electric Vehicles," *IEEE Access* 11 (2023): 127589-127607.
17. Zhu, Q., Kumar, A., Sundar, A., Egan, D. et al., "Development of a Series Hybrid Electrified Powertrain for a High Speed Tracked Vehicle Based on Driving Cycle Simulation," *SAE Int. J. Adv. Curr. Pract. in Mobility* 4, no. 4 (2022): 1403-1412, doi:https://doi.org/10.4271/2022-01-0367.
18. Kollmeyer, P., "Panasonic 18650PF Li-Ion Battery Data," *Mendeley Data* 1 (2018).
19. Pelletier, S., Jabali, O., Laporte, G., and Veneroni, M., "Battery Degradation and Behaviour for Electric Vehicles: Review and Numerical Analyses of Several Models," *Transportation Research Part B: Methodological* 103 (2017): 158-187.
20. Joshi, D., Ghimire, S., Shiuab, S., and Venkatasubramanian, M., "Computational Analysis of Online Oscillation Monitoring Algorithms," in *IEEE International Conference on Communications, Control, and Computing Technologies for Smart Grids*, Oslo, Norway, 2024, IEEE.
21. Mohamed, T., Kezunovic, M., Paudel, Y., Vittal, V. et al., "Automated Detection and Classification of Critical Power System Events Using ML on PMU Data," in *SGSMA 2024*, Washington, DC, May 2024.
22. Ghimire, S., Joshi, D., Venkatasubramanian, M., Torresan, G. et al., "Wide-Area Measurement Based Online Oscillation Alarming System at RTE," in *IEEE International Conference on Communications, Control, and Computing Technologies for Smart Grids*, Oslo, Norway, 2024, IEEE.
23. Timilsina, L., "Real-Time Degradation Abatement Framework for Energy Storage System in Automotive Application Using Data-Driven Approaches," PhD thesis, Clemson University, 2024.
24. Gonder, J. and Simpson, A., "Measuring and Reporting Fuel Economy of Plug-In Hybrid Electric Vehicles," *World Electr. Veh. J.* 1, no. 1 (2007): 134-141, doi:https://doi.org/10.3390/wevj1010134.
25. Sciarretta, A., Serrao, L., Dewangan, P.C., Tona, P. et al., "A Control Benchmark on the Energy Management of a Plug-In Hybrid Electric Vehicle," *Control Engineering Practice* 29 (2014): 287-298.
26. Hoang, P.H., Ozkan, G., Badr, P.R., Timilsina, L. et al., "Integrating Degradation Forecasting into Distribution Grids' Advanced Distribution Management Systems," *International Journal of Electrical Power & Energy Systems* 150 (2023): 109071.
27. Onori, S., Spagnol, P., Marano, V., Guezennec, Y. et al., "A New Life Estimation Method for Lithium-Ion Batteries in Plugin Hybrid Electric Vehicles Applications," *International Journal of Power Electronics* 4, no. 3 (2012): 302-319.
28. Paudel, S., Zhang, J., Ayalew, B., and Skowronska, A., "Charging Load Estimation for a Fleet of Autonomous Vehicles," SAE Technical Paper 2024-01-2025 (2024), doi:https://doi.org/10.4271/2024-01-2025.
29. Hoang, P., Ozkan, G., Badr, P., Timilsina, L. et al., "A Prognostic Based Control Framework for Hybrid Electric

Vehicles," SAE Technical Paper 2022-01-0352 (2022), doi:https://doi.org/10.4271/2022-01-0352.

30. Cenex, "Develop and Extend an Evidence-Based Technoeconomic Model of How V2G Will Be Viable within the UK," accessed August 23, 2023, https://www.cenex.co.uk/app/uploads/2022/06/EV-elocity-Final-Reportpublished.pdf.
31. Svarc, J., "V2G Explained: Vehicle-to-Grid Benefits," July 28, 2023, https://www.cleanenergyreviews.info/blog/v2g-explained-vehicle-to-grid-benefits.
32. The Economist, "Lithium Battery Costs Have Fallen by 98% in Three Decades," *The Economist* 134 (2021).
33. Timilsina, L., Moghassemi, A., Buraimoh, E., Arsalan, A. et al., "Impact of Vehicle-to-Grid (V2G) on Battery Degradation in a Plug-In Hybrid Electric Vehicle," SAE Technical Paper 2024-01-2000 (2024), doi:https://doi.org/10.4271/2024-01-2000.
34. PG&E, "Electric Vehicle (EV) Rate Plans," July 29, 2023, https://www.pge.com/enUS/residential/rate−plans/rate−planoptions/electric−vehicle−base−plan/electric−vehicle−base−plan.page.

ISSN 0148-7191